Lasers in Surgery and Medicine 18:345–357 (1996)

Light Distributions in a Port Wine Stain Model Containing Multiple Cylindrical and Curved Blood Vessels

Gerald W. Lucassen, PhD, Wim Verkruysse, MSc, Marleen Keijzer, PhD, and Martin J.C. van Gemert, PhD

Laser Centre, Academic Medical Centre, University of Amsterdam, 1105 AZ Amsterdam ZO (G.W.L, W.V., M.J.C.v.G.), and Faculty of Mathematics and Informatics, Delft University of Technology, Delft (M.K.), The Netherlands

Background and Objective: **Knowledge of the light distribution in skin tissue is important for the understanding, prediction, and improvement of the clinical results in laser treatment of port wine stains (PWS). The objective of this study is to improve modelling of PWS treated by laser using an improved and more realistic PWS model.**
Study Design/Materials and Methods: **Light distributions are calculated by the Monte Carlo method for various PWS blood vessel configurations, such as single and multiple vessels oriented horizontally, curved vessels, and "vertically" oriented vessels. Various vessel sizes and wavelengths are used.**
Results: **Our modelling confirms the concept of selective photothermolysis; 577nm laser light gives maximal deposited energy at the top side of the blood vessels closest to the skin surface and 585nm gives a more uniform energy distribution in the vessel. In the distribution of deposited energy multiple vessels mutually influence each other, because of "shadowing" of diffuse light.**
Conclusion: **Modelling PWS laser treatments with multiple vessels confirms the need for successive treatments of vessels layer by layer. The use of different wavelengths affects the local deposited energy profiles in the blood vessels. It predicts that the significance of 585nm laser light lies in the uniform energy distribution in the vessels rather than in gain in energy deposition with depth. The calculated light distributions provide a more realistic input for modelling thermal damage effects in PWS laser treatment and modelling of the epidermal response in thermal imaging of the PWS blood vessel structure.** © 1996 Wiley-Liss, Inc.

Key words: curved vessels, laser treatment, modelling, Monte Carlo, multiple vessels, oxyhemoglobin, pws, pulsed dye laser, vascular lesion

INTRODUCTION

Modelling of light distributions in skin tissues is important for predicting and understanding the results of laser treatment of vascular lesions such as port wine stains (PWS). In PWS patients, blood vessels progressively become ectatic with age, which gives the skin a pink to purple colour. Like other skin diseases, PWS often cause psychological stress [1]. The aim of the laser treatment is to injure the abnormal ectatic PWS vessels, which are replaced by vessels of normal size [2,3] resulting in normal coloured skin. Although good results (disappearing of the port wine stain) have been obtained with various laser systems, some PWS patients do not respond to the laser treatments for reasons that are currently not understood.

Accepted for publication April 2, 1995.

Address reprint requests to Dr. G.W. Lucassen, Laser Centre, Academic Medical Centre, University of Amsterdam, Meibergdreef 9, 1105 AZ Amsterdam ZO, The Netherlands.

The treatment is based on the idea of selective photothermolysis [2] by preferential absorption of laser light by oxyhemoglobin and deoxyhemoglobin in the erythrocytes of blood. This results in heating of the blood and by diffusion from the blood to the surrounding, also heating up the vessel wall. If the vessel wall temperature is kept long enough above a certain critical temperature (e.g., 70°C) [2], the vessel will be irreversibly damaged.

Modelling PWS laser treatment starts with simulation of light transport in a PWS skin model. Analytical solutions of the transport equation [4] that describe the light distribution are difficult to obtain, especially for complex geometries in inhomogeneous turbid media. Diffusion theory [5] and Kubelka Munk flux theory [6,7] have been used to calculate light fluence distributions in simplified skin models. These theories are accurate in the case of strongly scattering and weakly absorbing media, whereas in the case of dominant absorption over scattering Beer's law holds. Despite the fact that Monte Carlo (MC) programs to simulate light distributions are expensive in calculation time, such programs are powerful in that an exact solution to the transport equation can be obtained for complex geometries of, e.g., irregularly shaped blood vessels. The MC method is based on knowledge of optical parameters (absorption and scattering coefficients and anisotropy of scattering) of epidermis, dermis, and blood. We use optical parameters from the literature [8]. In the MC method [9] used here, *static* light distributions are calculated, i.e., it is assumed that the optical parameters do not change. In practice however, during laser treatment these parameters do change and also phase changes of blood heated above 100°C occur [10]. This means that the MC simulations give approximate (static) light distributions.

In the literature there are some MC studies using different skin models. Wang et al. [11] used a hybrid simulation model to calculate light distributions in simple layered geometries. The model makes use of diffusion theory to take over MC calculations far from boundaries, which speeds up the total calculation time. However, the disadvantage of the method is that in complex geometries with blood vessels embedded in the skin, diffusion theory is not accurate in and around vessels. For our purpose we cannot use this hybrid method. Keijzer et al. [12] reported on MC simulations of a single horizontally oriented cylindrical blood vessel in a layered skin model. In this study, optimization of wavelength and incident beam diameter were investigated in relation to minimal damage to epidermis and dermis. Miller et al. [13] have carried out MC simulations in a five-layer skin model including a discrete layer of whole blood to investigate the influences of variable finite beam widths and damage thresholds. Light distributions and initial thermal profiles were calculated for 577 nm and 585 nm irradiation. Verkruysse et al. [8] used MC simulations to study optimal wavelengths and maximal coagulation depths of a target vessel for various wavelengths and concentrations of homogeneously distributed blood above the target vessel in the dermis. It was shown that for longer wavelengths the light penetrates deeper for higher dermal blood concentration.

In all these studies noted above, rather unrealistic PWS vasculatures were assumed in the skin model such as a single vessel, discrete layer of blood oriented parallel to an epidermis and dermis layer, or a homogeneous distribution of blood. The objective of this study is to investigate light distributions in a more realistic multiple cylindrical blood vessel model of port wine stain skin in dependence of laser wavelength, size, and depth position of the blood vessels. We confirm the theoretical concept of photothermal selectivity by calculation of the total deposited energy in the vessel. We also study vertically oriented and curved cylindrical vessels with the curvature oriented perpendicular to the plane of epidermal and dermal layers. Such vascular geometries represent essential components of PWS vasculatures; to the best of our knowledge these have never been modelled. We simulate PWS laser treatments using the multiple cylindrical vessel geometry representing normal and PWS skin.

This article first describes the Monte Carlo method and then presents light distributions for several blood vessel geometries. Next, the effects of wavelength, shadowing, and penetration of the light are discussed, followed by a discussion of simulations of PWS treatments using the multiple vessel skin model.

MATERIALS AND METHODS

Monte Carlo Program

In this study a modified and extended version of the Monte Carlo (MC) program in Pascal code originally designed by Keijzer et al. [9,12] is used.

Model geometry. The skin is modelled by two plane parallel layers representing the epidermis and dermis of 60 μm and 2,400 μm thickness

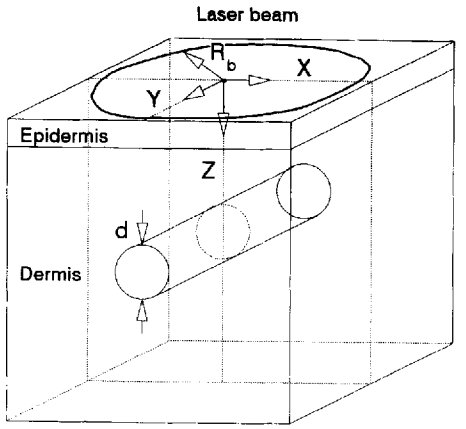

Fig. 1. Geometry of the skin model used in the Monte Carlo simulations. A uniform flat circular beam of radius R_b is incident normal to the skin, which is represented by two plane parallel layers of epidermal and dermal tissue. Cylindrical blood vessels can be implemented in the dermis.

(see Fig. 1). In our model we take melanin, the main epidermal absorber, to be homogeneously distributed in the epidermis. As in previous studies, blood is represented by the optical properties of oxyhemoglobin (HbO_2). Although the percentage of deoxyhemoglobin (Hb) at the normal tissue level is ~30% [14], the actual content of Hb in PWS is not known. Here, we use 100% HbO_2 as the absorbing blood chromophore. The optical properties are based on a hematocrit of 40%. We assume the oxyhemoglobin to be distributed homogeneously in the vessel. A Cartesian coordinate system is chosen with the z coordinate representing the skin depth and with the air-skin interface at $z=0$. The axis of the cylindrical collimated incident beam is along the z-axis. The beam radius is R_b. A three-dimensional grid of discrete boxes is defined in an array ($dx=dy=dz=20$ μm, with 50 boxes in the x and y directions and 125 boxes in the z direction).

Photon launching. In the MC program, light paths are simulated. We neglect polarization and interference effects. For cylinder symmetrical geometries, photon launching usually is done with a "pencil" beam at a single position $x=y=z=0$. This has the advantage of reducing total calculation time as light distributions in response to the pencil beam can be used to calculate the response to a finite beam by means of convolution. When the symmetry is broken, e.g., by inserting blood vessels into the model, the pencil beam method can no longer be used. Consequently, many photons must be used to obtain statistically significant results. In our MC program, photons are launched randomly in a circular flat beam profile at the skin surface ($z=0$) normal to the air/skin interface. To ensure launching a beam with a *flat* or *top hat* intensity profile, the initial photon position vector $r(x,y,z=0) = r(r\cos\phi, r\sin\phi, z=0)$ is uniformly distributed over areas πr^2, with $0 \le r \le R_b$, by sampling the radius r and the polar angle ϕ with the x-axis using random numbers. The sampling functions are given by [9]:

$$\xi_1 = \frac{\int_0^{r(\xi_1)} 2\pi r dr}{\int_0^{R_b} 2\pi r dr} = \frac{r^2(\xi_1)}{R_b^2} \quad \text{(1a)}$$

yielding

$$r(\xi_1) = R_b\sqrt{\xi_1} \quad \text{(1b)}$$

and the angle ϕ with the x-axis from

$$\phi(\xi_2) = 2\pi\xi_2 \quad (2)$$

where ξ_1 and ξ_2 are random numbers uniformly chosen from the range [0, 1] using a random generator procedure. The x- and y coordinates of the photon then follow from (1) and (2):

$$x = R_b\sqrt{\xi_1}\cos\phi(\xi_2) \quad \text{(3a)}$$

$$y = R_b\sqrt{\xi_1}\sin\phi(\xi_2) \quad \text{(3b)}$$

Random generator. The random generator procedure "ran3" adapted from Numerical Recipes in Pascal [15] is used. This procedure is much better than the intrinsic "random" procedure of Turbo Pascal, because ran3 uses double precision, has a large period, and still is relatively fast compared to other random number procedures.

Absorption and scattering. Absorption and scattering of photons occur at randomly distributed sites in the tissue. Each component of skin has its own set of optical parameters, viz. absorption coefficient (μ_a in cm^{-1}), scattering coefficient (μ_s in cm^{-1}), angular distribution of scattering with mean cosine (g) according to a Henyey-Greenstein phase function [16], and refractive index (n) (see Table 1). Above the epidermis we assume air with refractive index $n=1$, and beneath the dermis we assume a refractive index $n = 1.37$, equal to that of the dermis. At tissue and blood vessel boundaries, refraction and reflection coefficients are calculated with the Fresnel equations. By choosing a random number

TABLE I. Optical Properties of Epidermis, Dermis, and Blood* for Wavelengths 577, 585, and 590 nm as Used in This Study

Epidermis	$\mu_a[cm^{-1}]$	$\mu_s[cm^{-1}]$	g	n
577	18.5	480	0.787	1.37
585	18.0	470	0.790	1.37
590	18.0	470	0.790	1.37
Dermis				
577	2.2	131	0.787	1.37
585	2.2	129	0.790	1.37
590	2.2	129	0.790	1.37
Blood				
577	354	468	0.995	1.33
585	191	468	0.995	1.33
590	157	468	0.995	1.33

*Verkruysse et al. [8].

ξ_3 from [0, 1], the photon is reflected if ξ_3 is smaller than the reflection coefficient and transmitted otherwise. Critical angles for reflection are also accounted for.

Photon propagation. The photons propagate through the skin where each path length (Δl) is calculated from

$$\Delta l = -\frac{\ln(\xi_4)}{\mu_t}[cm] \quad (4)$$

with ξ_4 a random number chosen from [0,1], and $\mu_t = \mu_a + \mu_s$ is the total attenuation coefficient. This corresponds to a Poisson probability distribution for scattering and absorption. At interface crossings, path lengths are corrected for different optical coefficients of the media. In the case of transmittance to a new medium, the new path length $\Delta l'$ is calculated according to

$$\Delta l' = \frac{\mu_t}{\mu_t}\Delta l \quad (5)$$

where Δl, μ_t are the old path length and old total attenuation coefficient and μ'_t the new total attenuation coefficient.

Photon weights and scoring. In the MC program, the "weighted" method is used. The initial photon weight at launching is $W_0 = 1$. After each scatter event, a fraction (1 − a)W is absorbed, where $a = \mu_s/\mu_t$ is the local albedo of the medium and W the actual photon weight. Then, the actual photon weight W is reduced to a new weight aW. The absorbed fraction at position (x,y,z) in the corresponding box (dx,dy,dz) is scored in an array A[i,j,k]. These local absorbed fractions A[i,j,k] are used to calculate the local energy deposition D[i,j,k] (in [J/cm^3]). At a radiant exposure of E[J/cm^2] the local deposited energy is given by

$$D[i, j, k] = \frac{A[i, j, k]E \cdot \pi R_b^2}{N \cdot dV}[J / cm^3] \quad (6a)$$

where N is the total number of photons launched, dV = dxdydz the volume of a single box, and R_b is the laser beam radius. Converting the deposited energy into a light fluence ϕ [J/cm^2] is performed through division of D by the local absorption coefficient μ_a:

$$\phi[i, j, k] = \frac{D[i, j, k]}{\mu_a[i, j, k]}[J / cm^2] \quad (6b)$$

Reflection at the air-epidermis interface and transmittance at the maximum dermis depth are scored in two-dimensional (x, y) arrays. Photons that cross the lateral boundaries are scored as well. The total (direct and diffuse) reflection (R), absorption (A), and transmittance (T) are used to check the total energy balance (R+A+T=1). Furthermore, for each blood vessel, the total absorbed energy in the vessel is scored. Also, net light fluxes in x, y, and z direction as a function of z are scored along the z-axis (x = y = 0) in separate arrays using the direction cosines of scattering of the photon times the actual photon weight. These net light fluxes are used in the later discussion on shadowing effects behind vessels.

Photon termination. When the photon weight becomes less than a critical weight W_{cr}, a survival roulette is performed. A random number $\xi_5 \in [0,1]$ is generated and if $\xi_5 <$m, the weight is increased 1/m times, and the photon survives. Otherwise, the photon dies and the weight is absorbed. In this way termination of photon weight is accounted for properly. In our program, m = 0.1 and $W_{cr} = 0.0001$.

RESULTS

Blood Vessel Configurations

In this section, the results calculated for a number of different blood vessel configurations are presented. As a guide, a figure of the used configuration precedes the results. Starting from a single straight blood vessel and two straight blood vessels underneath each other, a vertically oriented blood vessel, a curved blood vessel geom-

etry, and multiple straight blood vessel geometries are used.

Straight Vessel

Figure 2a shows the single straight blood vessel geometry. Figure 2b,c displays three-dimensional plots of the deposited energy in a cross section (at $y = 0$) in the x-z plane of the geometry in Figure 2a, for the wavelengths 577 nm (Fig. 2b) and 585 nm (Fig. 2c). The deposited energy in the epidermis is larger than that in the dermis, due to a higher absorption of the former. Inside the vessel, light attenuation is observed. Since the anisotropy factor of blood is assumed to be high ($g = 0.995$) [4], the effective total attenuation constant $\mu_{eff} = \mu_a + \mu_s (1 - g) \approx \mu_a$, and light attenuation follows Beer's law. Diffuse light penetrates also into the vessel lumen from all directions around the vessel circumference.

The effect of different vessel diameters and laser wavelengths on the deposited energy profile inside the vessels is shown in Figure 3. Here, the deposited energy is displayed as a function of depth (z-axis) at $x = 0$. From this figure it is seen that at wavelength 577 nm ($\mu_a = 354$ cm^{-1} for blood), the deposited energy in the blood vessel steeply decreases, whereas at wavelength 585 nm ($\mu_a = 191$ cm^{-1}) and 590 nm ($\mu_a = 157$ cm^{-1}), these profiles are less steep. The longer wavelengths give a more uniformly deposited energy profile through the vessel cross section, although lower maxima are reached. These longer wavelengths give higher deposited energies in the centre of the large vessels compared with those at 577 nm. The same arguments are valid for laser wavelengths at the short wavelength side of the 577 nm oxyhemoglobin absorption peak. However, for these wavelengths the epidermal absorption is slightly increased due to the higher absorption of melanin with shorter wavelengths. Although the 60-μm vessel (Fig. 3a) is positioned a little deeper in the skin than the 120-μm vessel (Fig. 3b), the maximal deposited energy is virtually the same as that in the 120-μm vessel. Here, less amount of light available (decreasing fluence with depth) is compensated by diffuse light penetration all around the vessel. Furthermore, in the 60-μm vessel, the 577 nm deposited energy is larger than that at 585 nm and 590 nm throughout the vessel cross section. The contribution of diffuse light in addition to collimated light can be seen from the steepness of the deposited energy with the depth at the top of the vessel. In the smaller vessel this slope is less steep than in the larger vessel. Also,

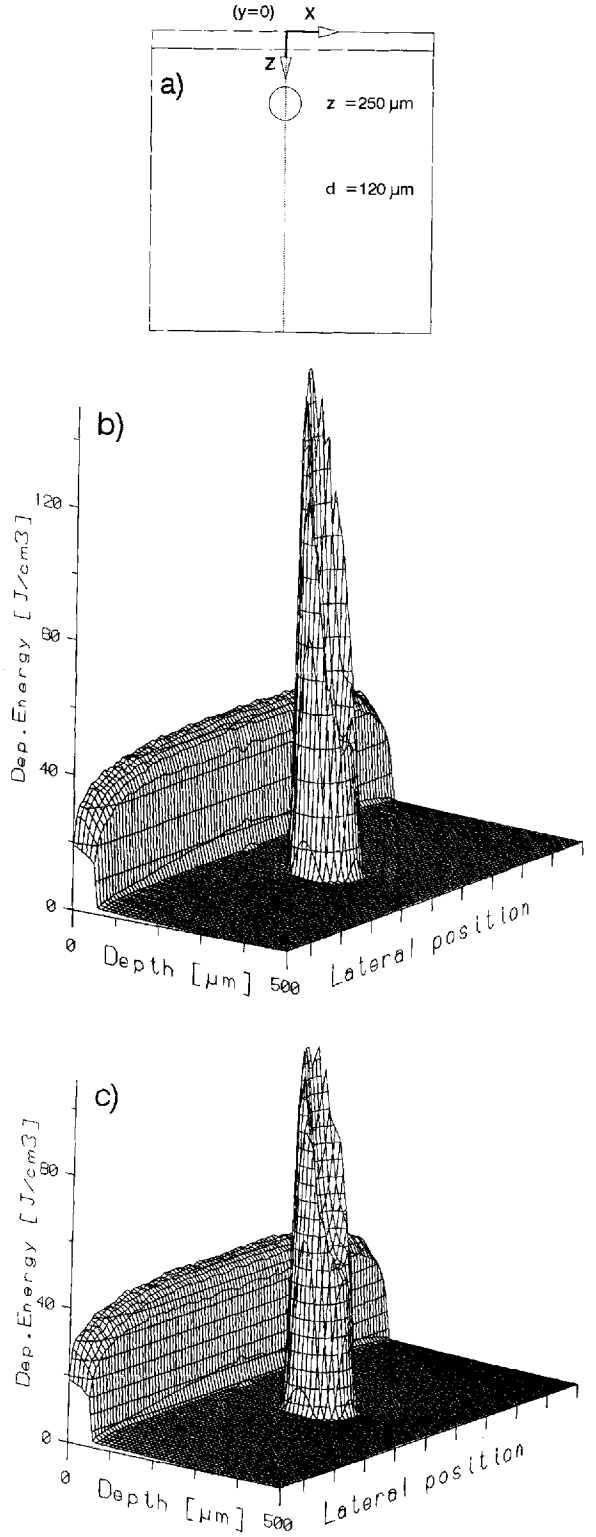

Fig. 2. (a) Single straight vessel geometry with centre at depth $z = 250$ μm and diameter d. (b) Plot of the deposited energy in a cross section at $y = 0$ through the xz plane for wavelength 577 nm, and (c) for 585 nm. The laser beam diameter is 1 mm. The deposited energy in the epidermis is larger than that in the dermis due to higher absorption of the epidermis.

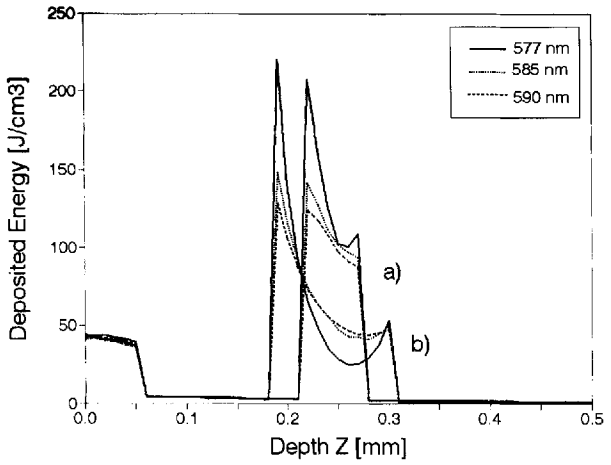

Fig. 3. Deposited energy versus skin depth z at x = y = 0 of the single vessel geometry (Fig. 2a) for wavelength 577 nm (solid), 585 nm (dotted), and 590 nm (dashed) (**a**) for vessel diameter d = 60 μm and (**b**) for d = 120 μm. Notice the contribution of diffuse light that can be observed at the bottom of the vessels.

at the bottom of the vessels, contribution of diffuse light is clearly seen by the increase in deposited energy (see, e.g., the 577 nm curves).

Two Straight Vessels

Figure 4a displays the geometry of two straight blood vessels. Deposited energy profiles versus depth for the two blood vessel configurations are presented in Figure 4b. The dotted line represents the deposited energy in a single vessel at 250-μm depth, the thin solid line in a single vessel at 500-μm depth, and the thick line in both vessels at 250-μm and 500-μm depth. The vessels have a diameter of 120 μm and the wavelength is 585 nm. Comparing the dotted and the thick line curves (first vessel at 250 μm), it is seen that the presence of the deeper vessel decreases the deposited energy in the upper vessel. Due to absorption of light in the deeper vessel, less diffuse scattered light (≈32%) reaches the upper vessel. Comparing the thin and thick lines (second vessel at 500 μm), it is seen that the presence of the upper vessel decreases the amount of light (≈22%) available to deposit in the deeper vessel. In this way the vessels mutually influence each other (shadowing) through the diffuse component of the fluence.

Shadowing Effects

A 2-D contour map of Figure 4b is displayed in Figure 5. Iso-deposited energy lines are plotted in steps of 0.1 J/cm^3. Significant shadowing behind the vessels occurs over a depth of about the vessel diameter. Since the dermis has a relatively large forward scattering anisotropy (g = 0.79), the overall energy transport is directed downward in the skin in the positive z-direction. However, by scoring the net light flux in the z-direction as a function of depth, we have noted fluxes in the negative z-direction just behind the vessels, indicating that the direction of energy transport is upward at the bottom of the vessel. Behind the vessel, diffuse scattering takes over again and flattening of the contour lines is seen. As can be expected, 577 nm gives a stronger shadowing effect than 585 nm because, in the latter case, more light is transmitted through the vessels. For a

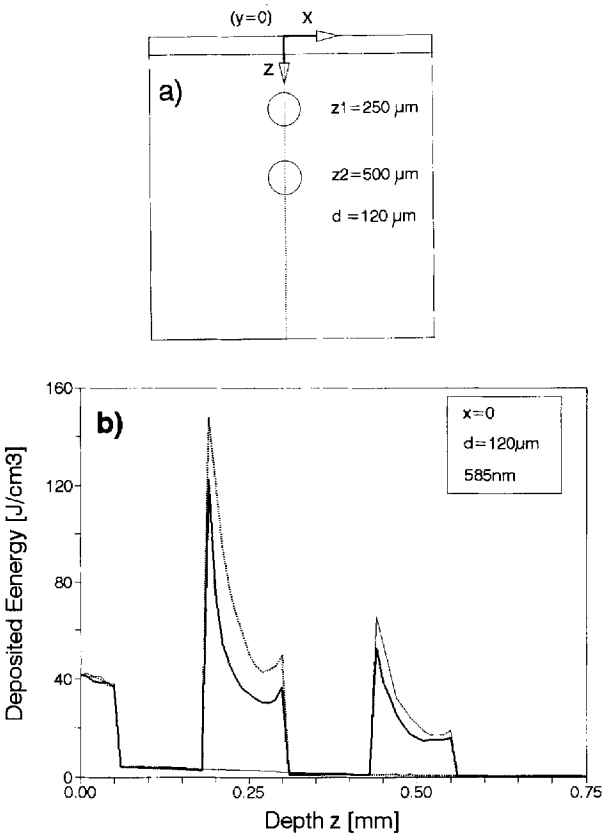

Fig. 4. (**a**) Two straight vessels at depths z1 = 250 μm and z2 = 500 μm with diameter d = 120 μm. (**b**) Deposited energy profiles versus depth of the geometry in (a) at 577 nm. The dotted line (first vessel) is for a *single* vessel at 250 μm depth, the thin solid line (second vessel) is for a *single* vessel at 500 μm depth, and the thick solid line is for *two* vessels at depths 250 μm and 500 μm, respectively. The differences between the dotted and thick solid lines are due to the presence of the deeper vessel, which diminishes the amount of backscattered light. The differences between the thin and thick solid lines are due to the presence of the upper vessel, which decreases the light fluence for the deeper vessel. Multiple vessels therefore mutually influence each other.

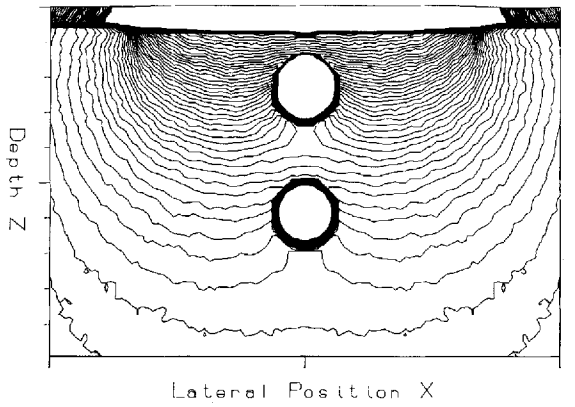

Fig. 5. Contour map of Figure 4 for wavelength 585 nm. Iso deposited energy lines are plotted in steps of 0.1 J/cm^3 to a cutoff at 5 J/cm^3. Shadowing behind the vessels is seen over a depth about equal to the vessel diameter. "Recovering" of the contour lines occurs due to light scattering in the dermis, which contributes to the diffuse component of the fluence.

large vessel diameter, the transmission of light through the vessel is less than for a small diameter vessel. The amount of scattered light that passes around the vessel also decreases with larger vessel diameter.

Total Deposited Energy in the Blood Vessel

To quantify the dependence of wavelength, vessel diameter, and vessel depth on the total deposited energy in the blood vessel, we introduce the ratio f of the total deposited energy in the vessel for wavelength 585 nm to that at 577 nm. In Figure 6a, this ratio f is displayed as a function of vessel diameter d, where the depth position z of the vessel centres is kept constant. For increasing vessel diameters, f gradually increases almost to 1, showing that for larger vessel diameters the total deposited energy in the vessel becomes virtually independent of the wavelength. In Figure 6b the ratio f is depicted as a function of vessel depth z at constant vessel diameter d = 120 μm (open squares) and d = 60 μm (filled squares). It is seen that f is almost constant, which means that the diffuse character of the light at these wavelengths does virtually not vary with depth. In the case of vessel diameter d = 60 μm, the average ratio is f = 0.78, and for vessel diameter d = 120 μm, the average ratio is f = 0.91.

Vertically Oriented Straight Vessel Geometry

In Figure 7 the deposited energy at the beam axis (x = 0) in a vertically oriented cylindrical blood vessel (Fig. 7a) is given as a function of skin depth (z) for two different vessel diameters d = 120

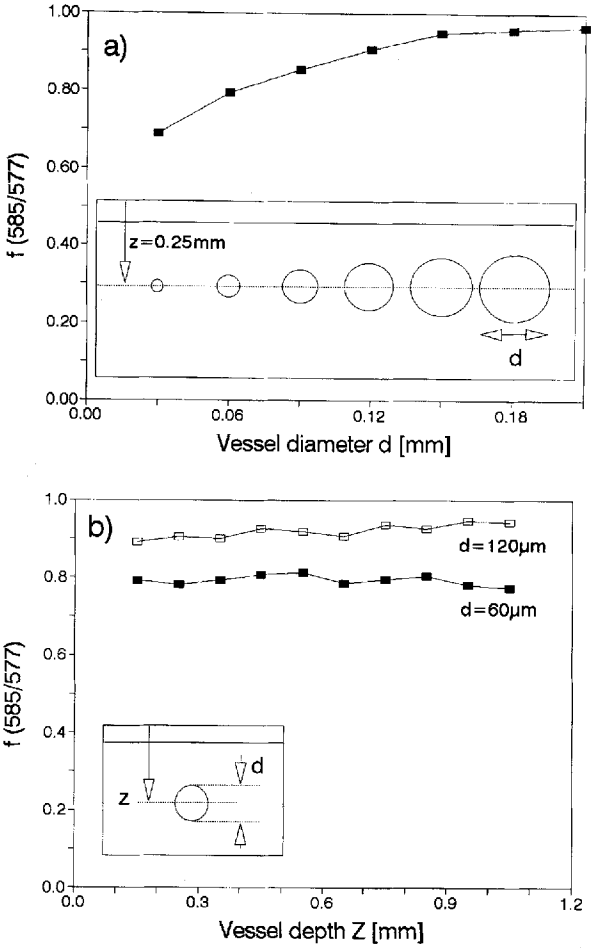

Fig. 6. Ratio f defined as the total deposited energy at 585 nm to that at 577 nm in the single straight cylindrical vessel configuration (of Fig. 2a) (**a**) as a function of vessel diameter d at constant vessel depth z = 250 μm, and (**b**) as a function of vessel depth with constant vessel diameter for d = 60 μm and d = 120 μm. In (a) it is seen that for increasing vessel diameter, the energy deposition at 585 nm approaches the deposited energy at 577 nm. In (b) it is seen that f is virtually independent of depth.

μm (Fig. 7b) and d = 200 μm (Fig. 7c), for wavelengths 577 nm and 585 nm. At the top of the vessel the collimated light is strongly attenuated following Beer's law. For larger z (deeper in the skin), diffuse light from all around the vessel contributes mainly to the fluence. It is seen that for 585 nm, the diffuse light contribution to the fluence in the centre of the vessel is larger than for 577 nm. At the vessel wall side (not displayed in the figure), the deposited energy is larger at 577 nm than at 585 nm.

Curved Vessel Geometry

The result for a curved vessel geometry (Fig. 8a) is given in Figure 8b. Energy is deposited

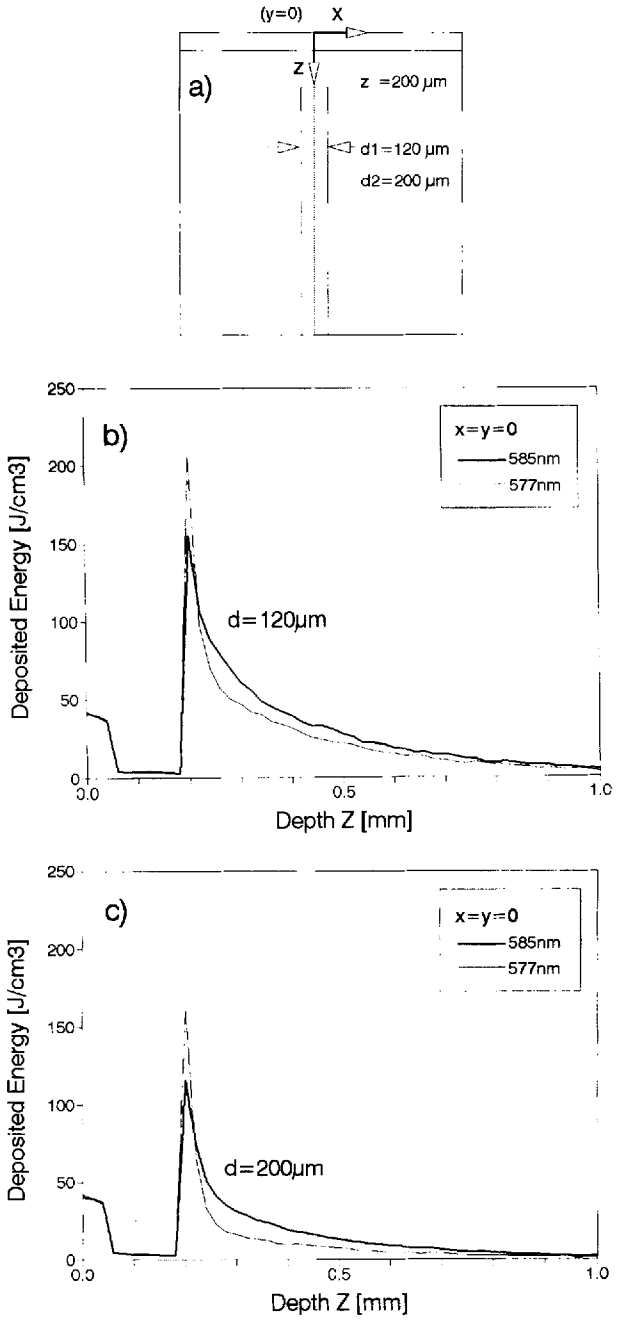

Fig. 7. (**a**) Vertically oriented straight vessel starting at z = 200 μm, with d1 = 120 μm, and d2 = 200 μm. Energy deposition along the z-axis for vessel diameter (**b**) *d1* = 120 μm and (**c**) for *d2* = 200 μm. The thin line represents a wavelength of 577 nm and the thick line a wavelength of 585 nm.

mainly at the top of the vessel. At 585 nm the deposited energy is distributed more evenly in depth over the curved vessel than at 577 nm. The smaller deposited energy in the "legs" compared to that in the top part of the curved vessel is due to two effects: orientation and depth. Because of their vertical orientation, the fluence in these vessel parts depends mainly on penetration of diffuse light. Furthermore, with increasing depth the available light fluence decreases due to absorption and scattering in the dermis.

Multiple Vessels

The multiple vessel geometry is given in Figure 9a. The deposited energy profiles are displayed in Figure 9b for wavelength 577 nm and in Figure 9c for 585 nm. The laser beam diameter is 1 mm. It is seen that most energy is deposited at the top vessels with highest values in the central two vessels. In the second layer, at depth 435 μm, the central vessel at x = 0 has less light absorption compared to its two lateral neighbours. This is due to shadowing of diffuse light by the two top vessels in the central region of the beam, whereas the neighbouring vessels receive a little more light at the edges of the laser beam. The vessels in the third layer receive even less energy. Note that the maximum deposited energy reached in the top vessels is about 120J/cm^3 (Fig. 9b). This is much less than the maximal value of deposited energy of 220J/cm^3 in a single vessel geometry at the same depth (see Fig. 2b, for 577 nm). In a multiple vessel geometry, the energy available in the laser beam is shared among the vessels resulting in lower maximal deposited energy.

The decreasing energy deposition in deeper vessels is a result of diminished light fluence and also shadowing effects, as in the examples given in Figures 4 and 5. Multiple vessels influence each other by diminishing the amount of light available for absorption by the others. Furthermore, the energy deposited in the vessels positioned at the edge of the laser beam is much less compared to the deposition in vessels at the centre of the laser beam. This is important with respect to the clinical concept of delivering laser pulses in an overlapping or nonoverlapping manner [17,18]. A slight overlap, 18% according to Dinehart et al. [18], of the pulses can give a more uniform clinical result because the decreased energy deposition at the edges of the laser beam induce less damage to the vessels. This obviously contradicts the observations of Tan et al. [19], who showed more injury at the edges of the spot than in the centre in guinea pig skin. However, although "thermal lensing" has been named [20] to cause this nonlinear laser tissue response, Tan's observations remain nonunderstood.

The deposited energy as a function of depth in a cross section through the vessels with centres

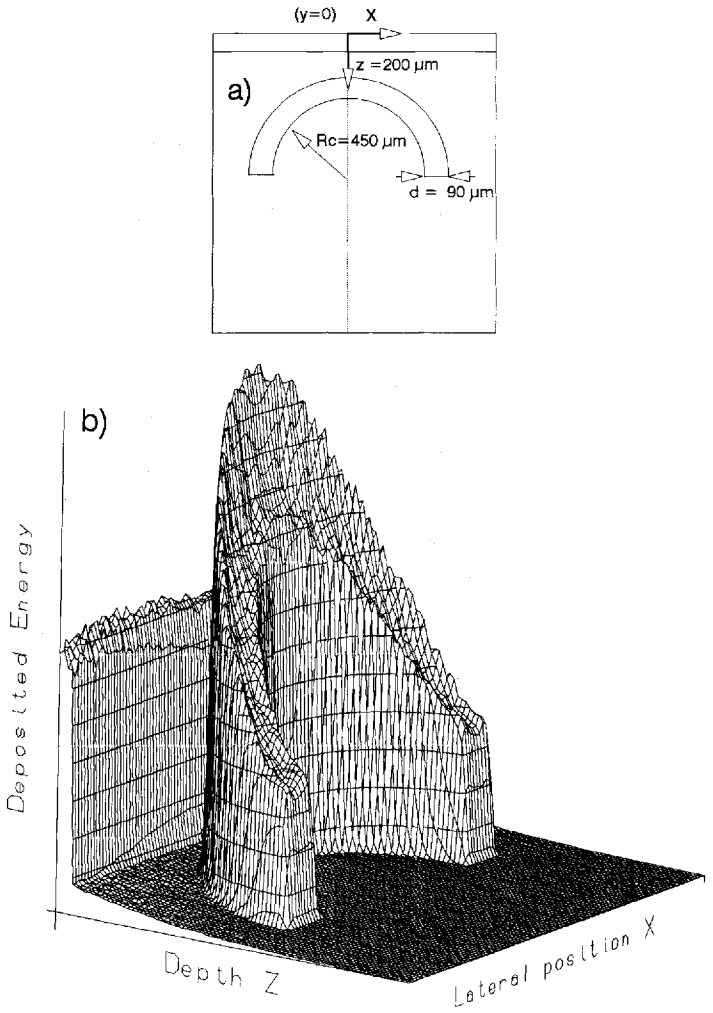

Fig. 8. (**a**) Curved vessel geometry with curvature $R_c = 450$ μm and diameter $d = 90$ μm. (**b**) Energy deposition in the curved vessel. The top part of the curved vessel receives most of the energy. The vertically oriented "legs" of such vessels receive mainly the diffuse part of the light fluence.

at $x = 135$ μm is given in Figure 10a for wavelength 577 nm and in Figure 10b for 585 nm. It refers to a simulated PWS laser treatment for the multiple blood vessel geometry (Fig. 9a) by assuming the concept of treating layer by layer where each treated layer of PWS vessels is replaced by a layer of "normal size" blood vessels of 30 μm diameter. This may seem rather large for normal vessels, but here we see that one treated PWS vessel may be replaced by three new "normal" vessels of 10 μm diameter [21]. Curve 1 shows the normal situation, i.e., before the first laser treatment on the layer of PWS vessels at 300 μm depth and with 120 μm diameter. It is assumed that the first treatment achieves irreversible injury of the PWS vessels at depth 300 μm and that these vessels are replaced by normal vessels. The resulting deposited energy behaviour is shown in curve 2. This is compared with the case that the treated vessels at depth 300 μm are totally removed and not replaced by new vessels (curve 3). It is seen that the deposited energy in the blood vessels at depth 570 μm are affected by the presence of the PWS vessels (curve 1), normal vessels (curve 2), or without these vessels at a depth of 300 μm (curve 3). Within the validity of this model the use of the different wavelengths 577 nm or 585 nm does not make much difference. With 577 nm, the top part of the deeper PWS vessel receives more energy, and with 585 nm laser light the profiles are more uniform.

In Figure 11b, the deposited energy is given

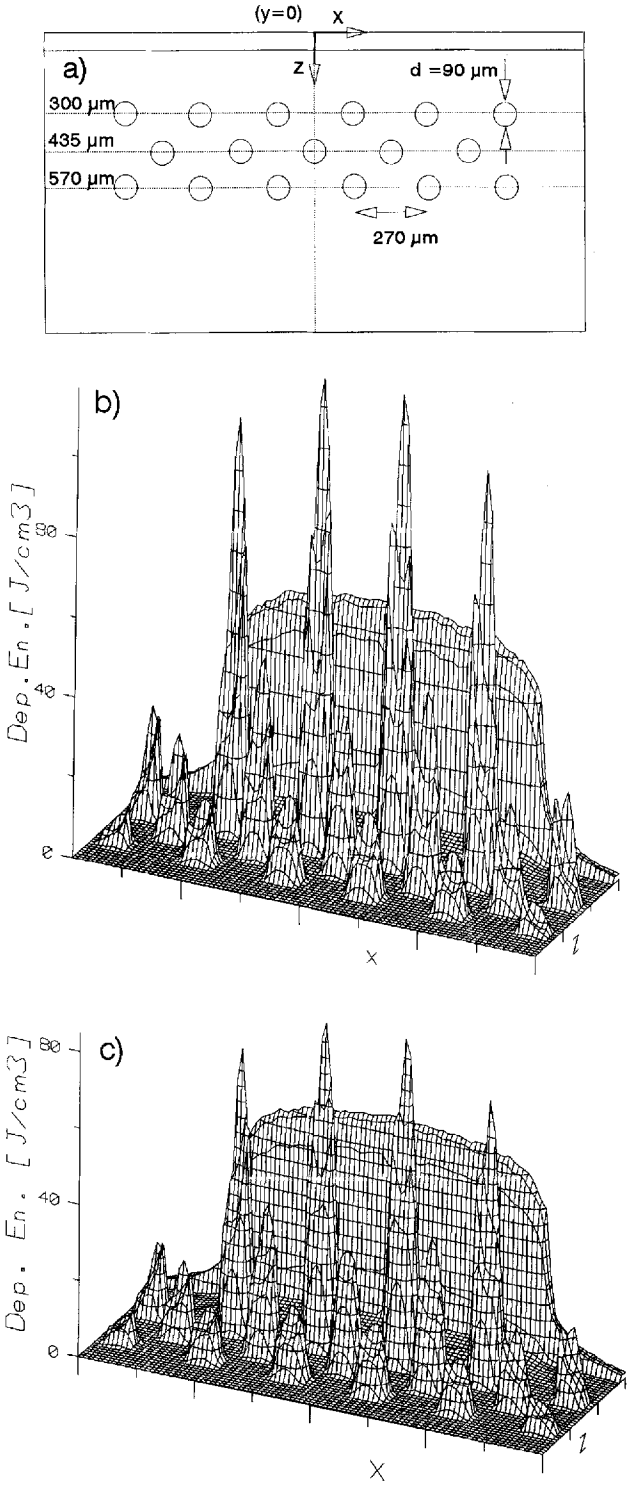

Fig. 9. (**a**) Geometry with 17 multiple straight vessels in three layers at different depths z = 300, 435, and 570 μm, and lateral spacing between the vessel centres 270 μm. (**b**) Energy deposition in a multiple blood vessel geometry for wavelength 577 nm and (**c**) for wavelength 585 nm. The laser beam diameter is 1 mm. The upper vessels receive most of the energy. The deeper vessels receive less energy by decreasing light fluence with depth and also by mutual shadowing of the vessels.

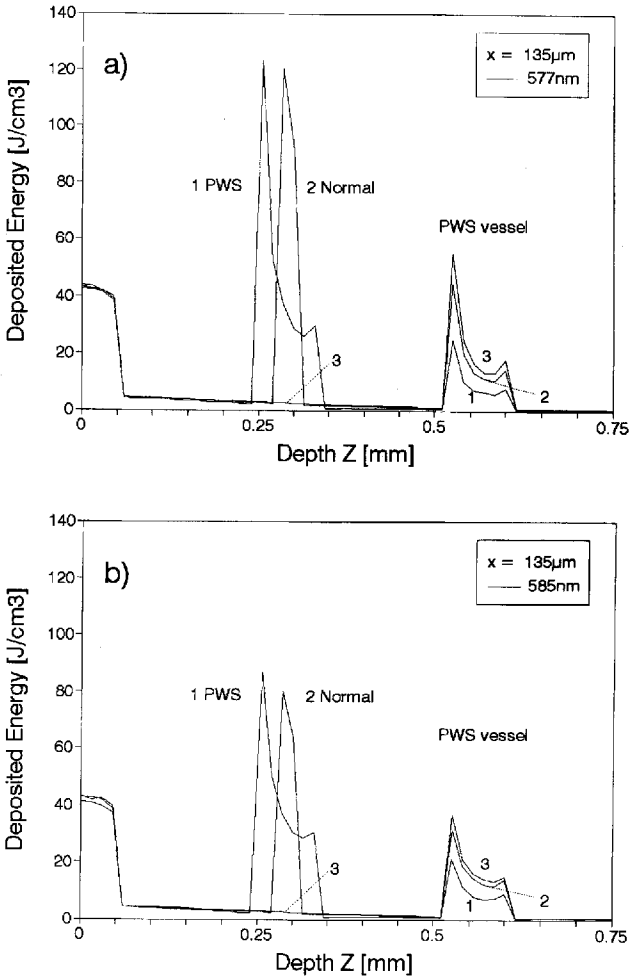

Fig. 10. Energy deposition versus depth in a cross section through the vessels at lateral position x = 135 μm (**a**) in the multiple blood vessel geometry of Figure 9a. The wavelengths are (**b**) 577 nm and 585 nm. First, the "normal" situation is modelled before the first (theoretical) PWS laser treatment of the blood vessels at depth 300 μm (denoted by 1 PWS). Second, the "treated" PWS vessels at depth 300 μm are assumed to be replaced by normal vessels of 30 μm diameter (2 normal). Third, case 3 refers to the situation that no new vessels replace the treated ones.

versus depth in the case of more layers of blood vessels at a regular depth and lateral spacing of 270 μm (see Fig. 11a). In this case, 585 nm laser light gives slightly higher deposited energy in the deepest layers of blood vessels (at 675 μm and 945 μm depth), compared to 577 nm. However, it is also seen from this figure that at these depths the deposited energy is much less than that at the top layers.

DISCUSSION

The results for a single straight cylindrical blood vessel with "large" vessel diameter (d > 120

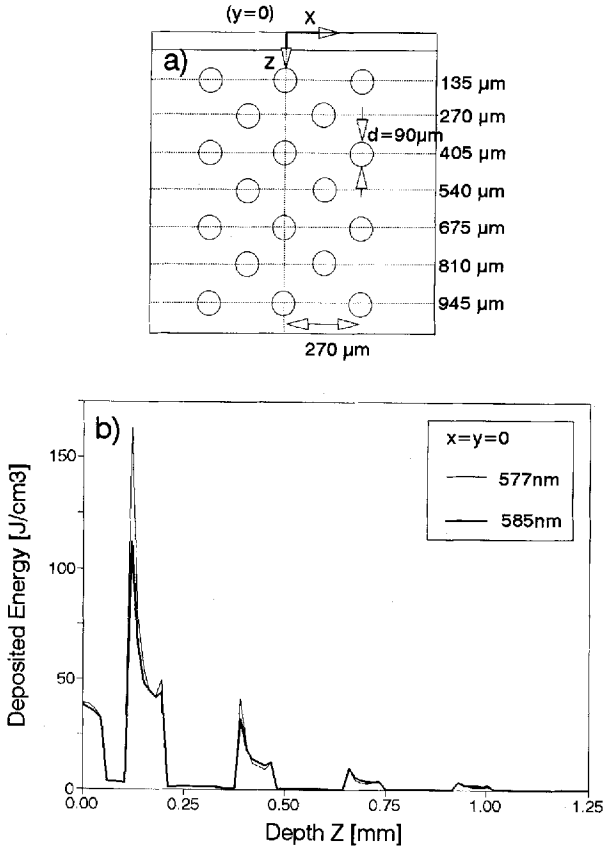

Fig. 11. (a) Multiple straight vessels with a regular depth and lateral spacing of 270 μm. (b) Deposited energy along the z-axis at (x = 0). The central depth of the first layer of vessels is 135 μm. It is seen that for 585 nm (thick line) the energy deposition in the deeper vessels is slightly higher than for 577 nm (thin line). However, the actual deposited energies at these depths are much less than those in the top layer of vessels.

μm) show that for laser light of 577 nm the energy is dominantly deposited at the top part of the blood vessel, whereas for larger (585 and 590 nm) or shorter wavelengths the deposited energy is more evenly distributed over the vessel cross section. For small diameter vessels (d < 60 μm), 577 nm gives an overall higher energy deposition than other wavelengths, which is due to the contribution of diffuse light penetrating the vessel all around. The diffuse component of the fluence is more important in deeper vessels in the dermis than in superficial vessels.

Concerning the dependence of wavelength, vessel diameter, and vessel depth on the deposited energy in the blood vessel, the results in Figure 6 show that at 577 nm the highest *total* energy is deposited in a single blood vessel no matter what vessel size or depth. We consider this an important finding because for the first time, it confirms the theoretical concept of selective photothermolysis [2], which implies that production of maximal heat in a whole *single* vessel requires using 577 nm. However, the total deposited energy at 585 nm becomes close to that at 577 nm with increasing diameter of the blood vessel, even though the absorption coefficients for oxyhemoglobin at 585 nm and 577 nm differ considerably (ratio is 0.54). The reason for this is that large vessels absorb almost all light inside the vessel. Using Beer's law, 90% of the energy is absorbed in 65 μm blood at wavelength 577 nm. For a blood vessel with a radius larger than 65 μm, the central part of the vessel thus hardly contributes to further absorption. This affects the effective absorption coefficient of the blood vessel, which decreases with larger blood vessel size. As discussed in relation to the results of Figure 5, the size of the blood vessel also influences the scattering behaviour of the light. As a consequence, the distribution of blood in discrete vessels rather than in layers or homogeneously distributed throughout the dermis can give different modelling results of light distributions and hence, can give different predictions of wavelength dependence of the light distributions in the skin.

Orientation of the Blood Vessel

From the results on the vertically oriented and the curved vessels (Figs. 7 and 8), it follows that the top part of the vessels receive most of the energy. The fluence in the deeper vertical parts mainly depend on the diffusely scattered part of the light that penetrates the vessel from all around. This means that these vertically oriented (parts of) vessels are more difficult to damage. Although there is a wavelength dependence for the penetration depth, as discussed earlier, the top parts of the vessels have highest probability to be damaged, independent of the wavelength used. When a full cross-sectional coagulation is needed to damage the whole vessel, 585 nm light gives a higher and more uniform energy deposition in the centre of the larger (PWS) vessels (and a more uniform distribution) than 577 nm. However, 577 nm gives higher energy deposition in the wall of the vertically oriented vessels than 585 nm.

Multiple Vessel Geometry

In the multiple vessel geometry, most energy is deposited in the top vessels (see Figs. 9–11). For PWS treatment this means that these vessels are injured first. Comparing the results for laser wavelengths of 577 nm and 585 nm in Figure 9

and 10, it is clear that at 585 nm lower maximal energy is deposited at the top of the vessels. At constant incident energy density of the laser, this means that a situation may occur that at 577 nm the top vessels are damaged, whereas at 585 nm the vessels would not be damaged.

Assuming that only the top most vessels are damaged irreversibly and that no new ectatic vessels take their place following long-term wound healing, and assuming a blood content of 1% for normal skin distributed in vessels of 30 μm diameter, our modelling shows similar deposited energy profiles in the top PWS vessels for both wavelengths. This means that successive laser treatments are needed to damage the PWS vessels and that the wavelength of choice is not very critical with respect to the depth of coagulation of the blood vessels. The significance of the use of different wavelengths lies in the different local deposited energy profiles.

If we take a damage criterion for coagulation of the blood vessel as in previous work [8,22], viz. the deposited energy at the top of the blood vessel should be more than or equal to the deposited energy at the epidermal/dermal junction, our results with the multiple vessel model suggest that vessels located deeper than ~0.5 mm would not be damaged. This may seem in contradiction with histological studies by Tan et al. [3,23], who found coagulated vessels as deep as 0.7 mm for 577 nm and 1.2 mm for 585 nm laser light. However, our modelling depends on the optical properties chosen. Since the optical properties for blood are reasonably known, we might have overestimated epidermal scattering and the melanin absorption in the epidermis since we assume melanin to be homogeneously distributed. By modelling discrete absorption sites (melanocytes at the basal layer), we expect that more laser light is transmitted to the dermis and blood vessels, which in return may lead to deeper coagulation of vessels.

CONCLUSIONS

For the present study we have focused on the relative effects of wavelength on energy deposition in the blood vessels. With 577 nm, the top part of the vessels may be damaged at lower energy densities of the laser than with 585 nm. However, with 585 nm laser light, the deposited energy is: (1) more uniformly distributed in the (large) vessels and (2) slightly higher for the deeper vessels compared with the energy deposited at 577 nm, although this gain in fluence is not significant compared to the much higher fluence in the top vessels. We predict that use of longer wavelengths than 577 nm may be profitable in the concept of treating more layers of vessels *simultaneously*. In order to damage the deeper PWS vessels, enough energy has to be deposited to heat the blood vessel to a critical temperature (e.g., 70°C [2]) where irreversible damage occurs. Using the longer wavelengths (e.g., 585 nm or 590 nm) with lower blood absorption, coefficients yield a more uniform and less depth-dependent deposition of energy in the blood vessels. However, to reach the damage threshold in the blood vessels, a higher incident energy density is necessary without damaging the epidermis and dermis. Practically, this can be done by precooling of the epidermis for a short time before the laser pulse [24], which lowers the temperature increase of the epidermis. It must be stated here the optimal strategy for PWS laser treatment is not a matter of wavelength alone. In this respect, the interplay between wavelength, incident energy density, and pulse duration has to be considered. We are currently investigating thermal diffusion and thermal damage modelling of PWS laser treatment using Monte Carlo simulations of light distributions in the multiple vessel geometry. Although in this report, we focus on PWS treatments, the multiple vessel Monte Carlo model can be used in other applications of photoselective thermolysis (vessels, pigmentations, tattoos, etc.) where the detailed understanding of *microscopic* light and energy distributions may help to match laser parameters with skin anatomy in order to optimize the clinical result.

ACKNOWLEDGMENTS

The authors thank Prof. Phil. H. Butler (University of Christchurch, New Zealand) for valuable discussions. This work was funded by the Dutch Technology Foundation (STW, grant AGN33.2954).

REFERENCES

1. Lanigan SW, Cotterill JA. Psychological disabilities amongst patients with port wine stains. Br J Dermatol 1989; 121:209–215.
2. Anderson RR, Parrish JA. Microvasculature can be selectively damaged using dye lasers: A basic theory and experimental evidence in human skin. Lasers Surg Med 1981; 1:263–276.
3. Tan OT, Morrison P, Kurban AK. 585nm for the treatment of port-wine stains. Plast Reconstr Surg, 1990; 86(6):1112–1117.

4. Ishimaru A. "Wave Propagation and Scattering in Random Media," vol. 1. New York: Academic Press, 1978.
5. Lakmaker O, Pickering JW, van Gemert MJC. Modeling the color perception of port wine stains and its relation to the depth of laser coagulated blood vessels, Lasers Surg Med 1993; 13:219–226.
6. Kubelka P. New contribution to the optics of intensely light scattering materials, Part 1. J Opt Soc Am 1948; 38:448–457.
7. Van Gemert MJC, Hulsbergen Henning JP. A model approach to laser coagulation of dermal vascular lesions. Arch Dermotol Res 1981, 270:429–439.
8. Verkruysse W, Pickering JW, Beek JF, Keijzer M, van Gemert MJC. Modeling the effect of wavelength on the pulsed dye laser treatment of port wine stains. Appl Opt 1993; 32:393–398.
9. Keijzer M. Light transport for medical laser treatments, PhD thesis, Delft, The Netherlands, 1993.
10. Tan OT, Morelli JG, Whitaker D, Boll J, Murphy G. Ultra structural changes in red blood cells following pulsed irradiation in vitro. J Invest Dermatol 1989; 92:100–104.
11. Wang L, Jacques SL. Hybrid model of Monte Carlo simulation and diffusion theory for light reflectance by turbid media. J Opt Soc Am A. 1993; 10(8):1746–1752.
12. Keijzer M, Pickering JW, van Gemert MJC. Laser beam diameter for port wine stain treatment. Lasers Surg Med 1991; 11:601–605.
13. Miller ID, Veitch AR. Optical modelling of light distributions in skin tissue following laser irradiation. Lasers Surg Med 1993; 13:565–571.
14. Asakura T and Festa RS. Hemoglobin, structure and function. In: E. Schwartz, ed. "Hemoglobinopathies in Children: Progress in Pediatric Hematology/Oncology," Vol. 3. PSG, Littleton. 1980.
15. Press WH, Flannery BP, Teukolsky SA, Vetterling WT. Numerical Recipies in Pascal. Cambridge: Cambridge University Press, 1989.
16. Henyey LG, Greenstein JL. Diffuse relaxation in the galaxy. Astrophysics 1941; 93:70–83.
17. Koster PHL, van der Wal AC, van der Horst CMAM. Histology of overlapping and non-overlapping pulsed dye laser pulses on normal human skin, International symposium on Biomedical Optics, Lille, France, 1994, no 2327-6.
18. Dinehart SM, Flock S, Waner M. Beam profile of the flashlamp pumped pulsed dye laser: Support for overlap of exposure spots. Lasers Surg Med 1994; 15:277–280.
19. Tan OT, Motamedi M, Welch AJ, Kurban AK. Spotsize effects on guinea pig skin following pulsed irradiation. J Invest Dermatol 1988; 90:877–881.
20. Motamedi M, Welch AJ, Cheong WF, Ghaffari S, Tan OT. Thermal lensing in biologic medium. IEEE J Quantum Electron 1988; 24:693–696.
21. Finley JL, Barsky SH, Geer DE. Healing of portwine stains after argon laser therapy Arch Dermatol 1981; 117:486–489.
22. Van Gemert MJC, Welch AJ, Pickering JW, Tan OT, Gijsbers GHM. Wavelengths for laser treatments of port wine stains and telangiectasia. Laser Surg Med 1995; 16:147–155.
23. Tan. OT, Murray S, Kurban A.K. Action spectrum of vascular specific injury using pulsed irradiation. J Invest Dermatol 1989: 92:868–871.
24. Nelson JS, Milner TE, Anvari B, Norvang LT, Tran NH, Tanenbaum BS, Svaasand LO. Dynamic cooling of the epidermis during laser port wine stain therapy. Lasers Surg Med 1994; 6:48.